# Electronic Properties of Junctions Between Aluminum and **Poly(3-(2,5-dioctylphenyl) thiophene) (PDOPT)** thin films.

A thesis presented to the
School of Graduate Studies
Addis Ababa University

In Partial Fulfillment
of the Requirements for the Degree
of Master of Science in Physics

**By**
**Getachew Tizazu**

**June 2001**
**Addis Ababa**

**ADDIS ABABA UNIVERSITY**
**SCHOOL OF GRADUATE STUDIES**

## Acknowledgement

First of all, I would like to thank sincerely my advisor Dr. Bantikassegn Workalemahu for his unlimited and constructive guidance. The convenient working environment he has created with the necessary materials is greatly appreciated.

I would like to thank also physics department of Addis Ababa University.

I greatfully acknowledge the financial support from the International Program in the Physical Science (IPPS).

Special thanks goes to Tesfaye Ayalew and Abay Gadisa who introduced me about the laboratory work and who gave me fruit full suggestions during the whole work.

# Abstract

This thesis is based on the study of the electrical properties of the Sckottky barriers formed between aluminum and spin-coated films of PDOPT in the form of Al/PDOPT/PEDOT-PSS/ITO and Al/PDOPT/ITO sandwich structures, respectively. From the I-V characteristic, the rectification ratio, diode quality factor and barrier height have been obtained for both Al/PDOPT/PEDOT-PSS/ITO and for Al/PDOPT/ITO structures.

The Cole-Cole plot of the complex impedance spectra for Al/PDOPT/ITO exhibits part of a single bias voltage-dependant semicircle, which is a characteristic of most metal semiconductor junctions. The complex impedance spectra of Al/PDOPT/ PEDOT-PSS/ITO device showed two partially overlapping semicircles at reveres bias voltages which revealed the existence of thin insulating interfacial layer at metal/polymer junction.

## CONTENTS

## List of figures

## List of tables

# 1. INTRODUCTION

Modern electronics is built upon the foundation of a well-established semiconductor technology, which is based on inorganic semiconductors such as silicon. But the use of these inorganic materials for electronic and optoelectronic devices require high manufacturing cost. After the discovery that conductivity of conjugated polymer, polyacetylene, can be varied from insulating through semiconducting to metallic regimes [1], researches on the application of conducting polymers are being conducted to find an alternative to the conventional inorganic materials in many applications because of their semiconducting properties, diversity, ease of fabrication, and potentially low cost.

These organic polymers are large molecules made up of the repetition of small, simple, chemical units with alternating single and double bond known as conjugation. The exact molecular weight for a molecule to be called a polymer is a subject of continued debate. Often polymer scientists put the number at about 25,000g/mol or more. This is the minimum molecular weight required for good physical and mechanical properties for many important polymers [2]. Polymers are often considered insulators. Although this is true for saturated polymers, the situation for conjugated polymers is different. In conjugated polymers the $sp^2$ hybridization leads to one unpaired electron which results in alternating single and double bonds along the back bone of the chain. This alternating single and double

bonds (conjugation) is the origin of the interesting electronic properties of conducting polymers.

The first conjugated polymer to be tested as a semiconductor in a diode was polyacetylene [3]. But subsequent improvements in synthesis, stability, and processability have lead to numerous studies on polymeric diodes. Undoped or doped conjugated polymers, such as polythiophene and its derivatives have been studied as Schottky junction diodes [4-7], metal-Insulator-Semiconductor diodes [8], light-emitting diodes [9], field effect transistors [10]) and photoelectrochemical cells [11,12]. There are also other conjugated polymers that have been studied. For instance, polypyrrole as Schottky barrier diodes [13-16], solar cells [17], and polyaniline as Schottky barrier diodes [18], and solar cells [19]. All these studies have shown that these conjugated polymers do have semiconducting properties that can be used in device fabrications.

Recently derivatives of polythiophene have attracted considerable attention because of their stability, processability, quality, and ease of fabrication. They are soluble in common organic solvents and melt processable [20]. Poly[3-(2,5-dioctylphenyl) thiophene] (PDOPT) is one of the polythiophene derivatives, that we used as an active conjugated polymer for the device that we studied.

In this thesis electrical properties of junctions between a low work function metal (aluminum) and an organic polymer, PDOPT, spin coated on Indium Tin Oxide (ITO) in the form of (Al/PDOPT/ ITO) and PDOPT spincoated on Poly(3-,4-

ethylenedioxythiophene)-Poly(4-styrenesulfonate) (PEDOT-PSS) film initially spincoated on ITO in the form of (Al/PDOPT/PEDOT-PSS/ITO) sandwich structures were studied. Both polymeric films are extremely thin and their electrical properties differ considerably from that of melt-processed thick films [20]. The current-voltage measurements as well as the complex impedance spectroscopy are used for the characterization of this structure. We used thermionic emission theory to interpret the J-V characteristics and the complex impedance is measured and plotted as a Cole-Cole plot and analyzed.

## 2.Conjugated Polymers

Polymers are macromolecules consisting of a great number of repeating units, which are coupled to each other by covalent bonds to form a long chain. These repeating units can be any group of atoms, however, we consider only organic polymers, where the backbone consists of only carbon atoms. Most organic polymers that have side chains are soluble in organic solvents. The solvents easily evaporate upon spin-coating, leaving thin uniform films on a substrate [21].

Polymers in their neutral form are insulators due to the large band gaps and strong electron-phonon coupling, which are characteristics of these materials [22]. They are often considered uninteresting from electronic point of view until 1970's [23]. They were only used commonly for plastic bags, paints, adhesives, cloth and insulating electrical materials. Although this is true for polymers, which contain saturated carbons in which their backbone consist of $sp^3$ hybridized orbitals, the situation in conjugated polymers is much more interesting. In fact the conjugated structure is the origin of the interesting electronic properties of conducting polymers. Their backbone consists of $sp^2$-hybridized carbons and show semiconducting properties.

In conducting polymers the $sp^2$ hybridization leads to one unpaired electron per carbon atom. Out of the remaining three valence electrons, two form a rotationally symmetric $\sigma$-bonds with neighboring carbon atoms, while the remaining one bonds with hydrogen or another hetroatom. These $\sigma$-bonds are in a plane

one bonds with hydrogen or another hetroatom. These σ-bonds are in a plane forming $120^0$ [24] to each other. The main chain of conducting polymers is held together by these rotationally symmetric σ–bonds. The remaining electron has symmetry of a $2p_z$ orbital, which is perpendicular to the plane formed by the other three.

Two adjacent $2p_z$ orbitals interact and form π-bonds which are not rotationally symmetric. Rather they are perpendicular to these σ-bonds. Because of this, it forces the molecule into a planar conformation to maintain maximum overlap between each pair of $P_z$ orbitals. The most interesting properties of organic materials arise from the delocalization of π–orbital. That is, the electrons in the π-band are not concentrated along an axis between the two atoms but are shared in a region of space both above and below the plane defined by $sp^2$ orbitals. On the other hand, if the $2p_z$ orbitals don't overlap along the backbone, due to being orthogonal to each other, the resulting π–bond will be flat, which results in localized electronic states.

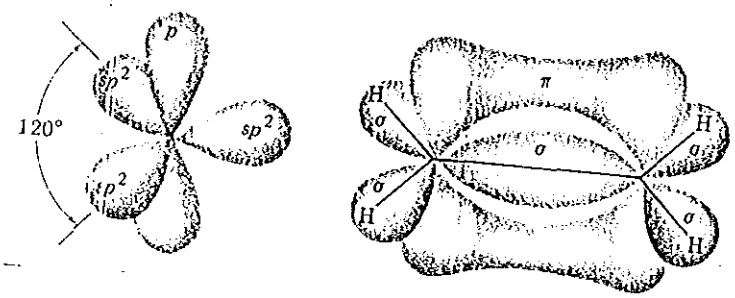


Fig.2.1 Representation of σ and π- bonds [24].

These molecules have a strict alternation of single and double bonds, i.e., $\sigma$ and $\sigma+\pi$ bonds respectively. Double bonds are strong, localized, and shorter, where as single bonds are weak, delocalized, and longe. Due to strong and localized nature of double bonds, conductivity of conjugated polymers along the chain is very small, leading them to be insulators or semiconductors. There exist different kinds of conjugated polymers out of which some are depicted below in Fig.2.2.

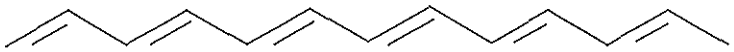

a)

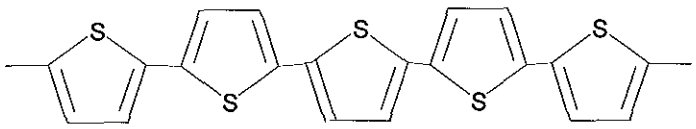


b)

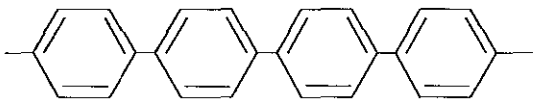

c)

Fig.2.2. Some chemical structures of conjugated polymers, a) *trans*-Polyacetylene, b) Polythiophene and c) Poly (*p*- phenylene).

Most conjugated polymers are synthesized from hetrocycles by the addition of side chains. For instance, PDOPT, PEDOT, PTOPT and POPT are a few derivatives of polythiphene. The sulfur in polythiophene increases the interchain coupling through d-orbital overlap and thereby improves the interchian transfer of charge carriers necessary for conductivity [22].

## 3. Electrical Properties of Conjugated Polymers

From energy point of view, we can divide conjugated polymers into two, i.e., polymers having degenerate ground state energy and polymers having non-degenerate ground state energy. In the degenerate case, the change in the order of single and double bonds doesn't result in a difference in the ground state energy. So from quantum chemical point of view they are two-fold degenerate, where as in non-degenerate case, the molecular structure favors a certain alternating order only. For the sake of simplicity, we consider two examples, polyacetylene (PA) and polythophene (PT) for degenerate and non-degenerate respectively.

a)

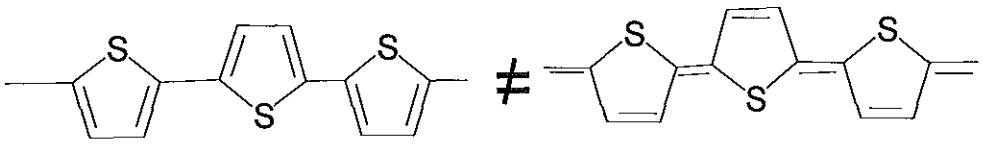


b)

Fig. 3.1 Structural diagrams for *trans*-polyacetylene showing the two equivalent phases (a), and for polythiophene showing Quinoidal and Aromatic structures (b).

Polyacetylene is a linear polymer consisting of weakly coupled CH units forming a one-dimensional lattice. It has the most regular and symmetric structure of all conducting polymers. Moreover the concept developed for polyacetylene can be generalized for all polymers whether degenerate or non-degenerate. It has only a main chain of covalently bonded carbon atoms except one hydrogen attached to every carbon atom.

### 3.1. Peierls Distortion

Quasi-one-dimensional metals tend to distort spontaneously [25] such that the spacing between successive atoms along the chain is modulated with period $2\pi/a=2\pi/k_F$, where $k_F$ is the fermi wave number. When the band is half filled the tendency toward symmetry breaking is strong, and the distortion leads to the pairing of successive atoms along the chain or dimerization. This dimerization opens a gap at the fermi surface, which is the property of semiconductors or insulators.

If we consider that polyacetylene is an extended chain with a bond angle of $180^0$, then it will be a one-dimensional lattice with equal length of C-C bonds. Carbon has four valence electrons so one electron is not involved in the covalent bond. A chain with equidistant carbon atoms would have one free electron per unit cell making a half-filled metallic band. So polymers like any other one-dimensional solids undergo a metal-to-insulator transition because of lattice distortion. The

dimerization doubles the size of the unit cell from one C-H unit to two, which reduces the first brillouin zone to half its previous size, i.e., the fermi wave vector values from $\pi/a$ to $\pi/2a$, and opens a gap ($E_g$). Hence conjugated polymers become insulators or semiconductors in case of lower value of Eg, as depicted in Fig.3.2(d). This is the case in which the conjugated polymers are dimerized.

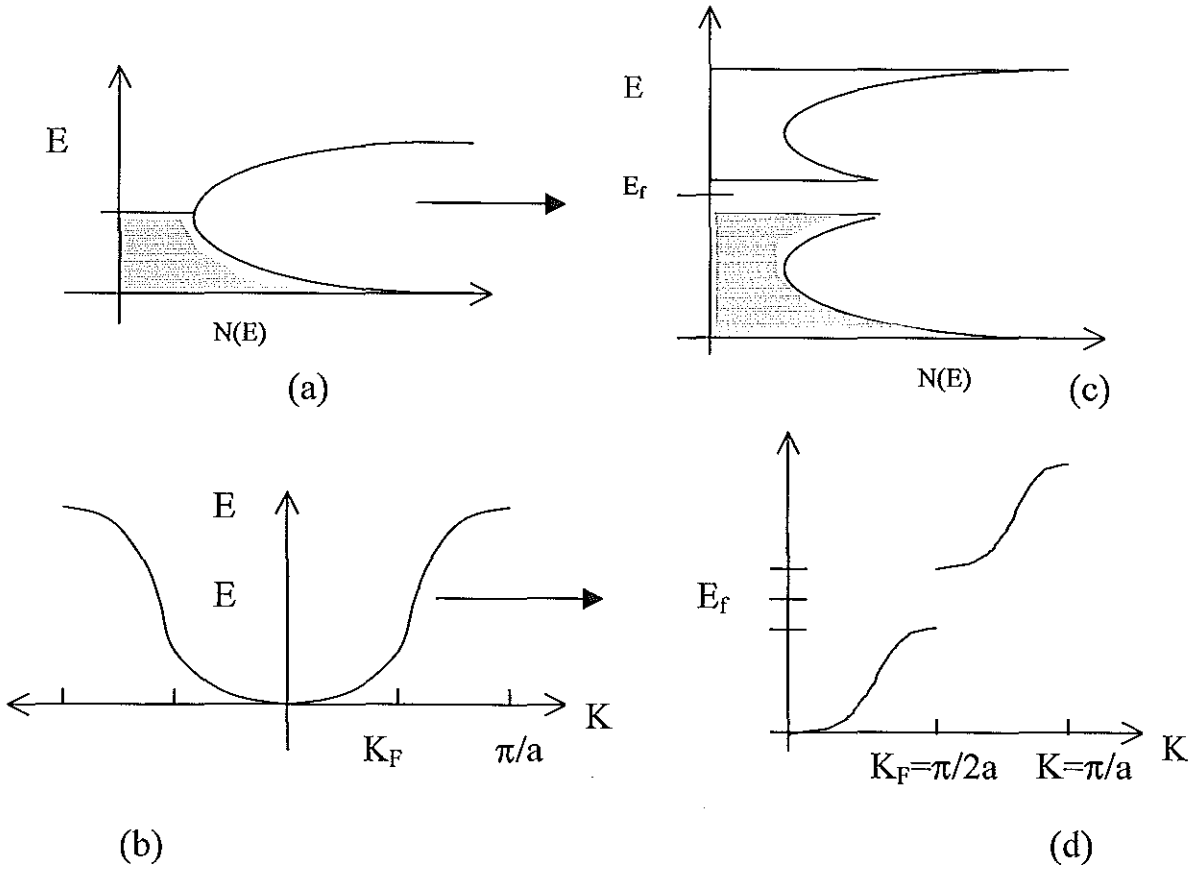


Fig.3.2 The reduction of the brillouine zone into half due to dimerization. N(E) is density of states.

In the case of undimerized polymers, the free electron of each carbon atom is "equally" distributed over the neighboring carbon atoms. There is no single and double bond alternation. Such unstable polymers behave like metals, see Fig.3.2 (a,b).

Several conjugated polymers have $E_g$ varying from 1ev to 4ev. For instance, from optical absorption spectrum, energy gap of Polyacetylene is 1.7ev [22]. But most other conjugated polymers have values higher than 1.7ev. Due to this, their intrinsic conductivity is very low. To get a considerable conductivity they should be doped. Doping of polymers is different from doping of inorganic materials. In the case of polymers doping causes the local geometry modification of the chain that affects the electronic structure by inducing electronic states in the energy gap. These levels are all due to charge-transferred-induced modifications of the $\pi$-system of the polymer and in that sense are intrinsic to the polymer [26,27].

## 3.2 Charge Carriers

In conventional inorganic semiconductors, conductivity is due to the presence of electrons and holes. In conducting polymers the conductivity is due to defects in conjugation.

There exist two energetically equal forms of polyacetylene in its ground state, Fig. 3.3 (a, b). If the two phases exist in the same chain, there will be a defect,

which separates the bond alternation, as shown in Fig. 3.3 (c). This defect is usually called soliton [28-30]. Since the chain is energetically equal the solitons can move freely along the backbone of polymer polyacetylene. A single soliton in polyacetylene can be accommodated per fourteen carbon atoms along the chain [31]. Solitons conserve charge and energy as water waves (also called solitons from solitory waves) conserve shape and energy [32]. But there is a difference in passing through each other, water waves can pass through while solitons in polymers cannot.

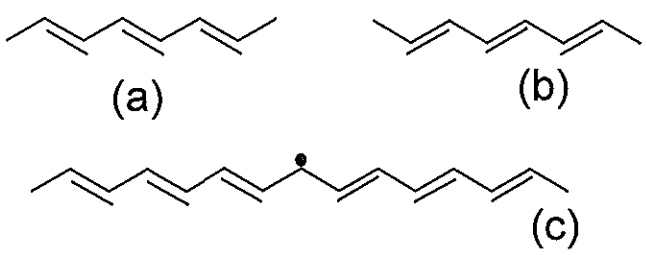


Fig.3.3. (a) and (b) are two energetically equal structures of PA, (c) is the formation of a soliton due to a misfit of the two structures in a single chain.

These defects (solitons) are neutral since the carbon atom at the soliton site is electrically neutral. This soliton is a dangling (unbounded) electron. It produces a new electronic state at the band gap. This state carries a reversed spin-charge relationship. Solitons can be generated by means of chemical, electrical, exposure to light or charge injection.

During doping the defect is more sensitive than the rest of the chain. In the process of doping, if two electrons compensate the carbon ion, the defect (soliton) will be negatively charged. On the other hand if no electron compensate the carbon ion, it will be positively charged. In such cases the defects are called negative soliton or positive soliton, respectively, as shown in Fig. 3.4.

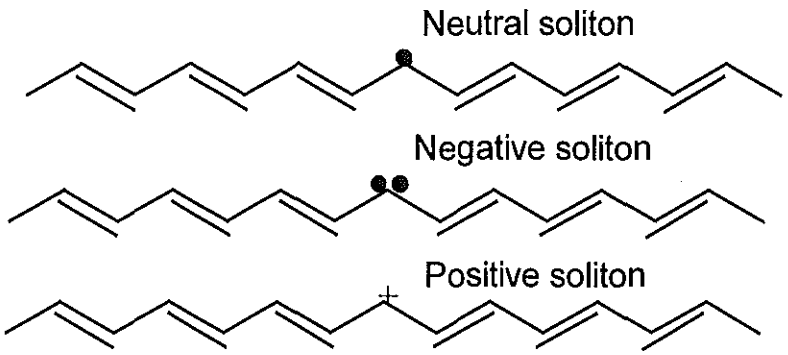


Fig. 3.4 Solitons in *trans*-polyacetylene.

Doping conjugated polymers will create states in the forbidden gap. If the doping level increases, the electronic states with in the gap will form soliton band. At about 30% of doping level these states expand and fill the gap resulting in metallic conductivity [22]. Electronic states formed within the gap by these three types of defects, i.e., neutral, negatively charged, and positively charged, are illustrated bellow in Fig. 3.5.

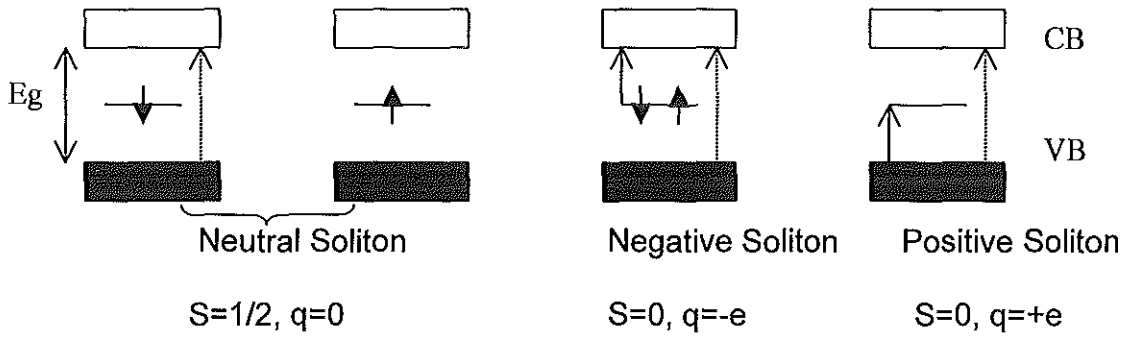


Fig.3.5 Schematics of the energy band diagram of polyacetylene with solitons. Dashed and thin solid arrows indicate the interband and subgap transitions, respectively where as the short arrows represent electron spins.

Solitons may be created in polyhetrocyclic polymers such as polypyrrol and polythiophene. The soliton site separates the polymer chain into aromatic and quinoidal segments as shown in Fig. 3.6. These are two different bond alternations. The aromatic has lower energy while the quinoidal has higher energy. The solitons in non-degenerate polymers are unstable, since creation of solitons requires two-fold degeneracy. This is because the lattice force pushes it to change the higher energy quinoidal to lower energy aromatic [33].

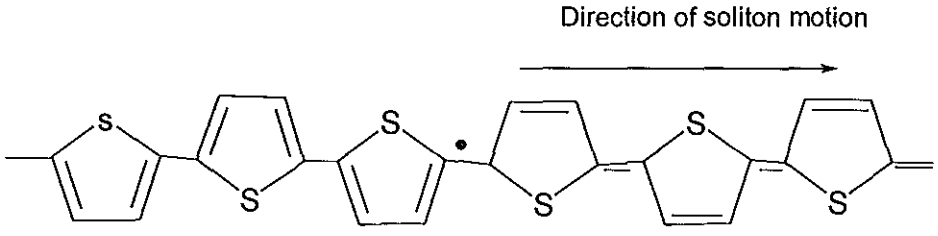


aromatic quinoidal

Fig.3.6. Unstability of solitons in non-degenerate polymers.

To create stable defects in non-degenerate polymers, we should have double-bound defects called polarons. Here one of the defects must be neutral while the other is charged negatively or positively. If the other is negatively charged the bound defect will be an electron polaron, where as if it is positively charged it will be a hole polaron. These charge carriers are generally formed from charge transfer. If the dopant is an acceptor, charge transfer takes place from polymer to acceptor, where as if it is a donor, charge will transfer from dopant to polymer. Here an acceptor ($A^-$) and donor ($D^-$) counter ions reside between polymer chains.

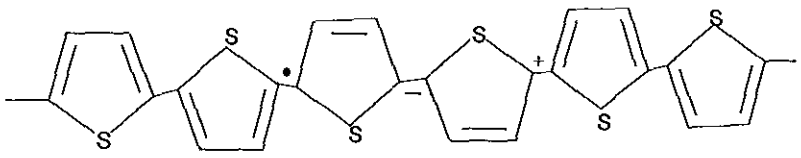

a)

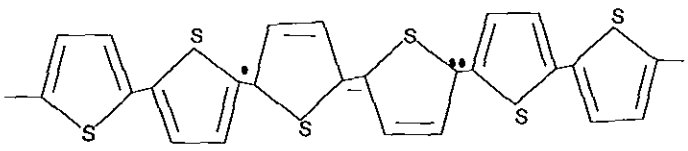

b)

Fig.3.7 (a) Positive polaron, (b) Negative polaron.

If two polarons exist in one chain, they will move towards each other to minimize the energy and form bipolarons. Here the neutral defects interact and form

a bond while the charged solitons remain at a minimum separation of four rings [27,34]. So bipolarons are doubly charged spinless charge carriers. Formation of bipolarons is due to the fact that formation energy of bipolarons is favorable over the existence of two polarons, i.e., energy of the two polarons is greater than energy of a bipolaron ($E_b<E_p$, where $E_b$ is energy of bipolaron and $E_p$ is energy of polaron) [35]. That is, electron-electron coulomb correlations are relatively weak compared to the energy difference between a bipolaron and a pair of isolated polarons. If two of the defects are positive, the existing doubly charged defects are hole bipolarons, where as if both of them are negative, it will be electron bipolaron. There is a considerable possibility that an electron and a hole polarons interact to yield a bound electron-hole pair called an exciton, see Fig. 3.8.

$P^+ + p^+ \rightarrow P^{++}$ hole bipolaron

$P^- + P^- \rightarrow P^{--}$ electron bipolaron

$P^+ + P^- \longrightarrow P^{-+}$ exciton

Excitons can be produced by photoinjection. That is, an incident photon is absorbed by an electron in the valence band and jumps to the conduction band leaving a hole in the valence band. These electron hole pairs in polymers created as a result of photon absorption are bounded together. This mechanism is photogeneration of charge carriers. Bipolarons may be formed directly in addition to recombination of two polarons at high doping level.

a)

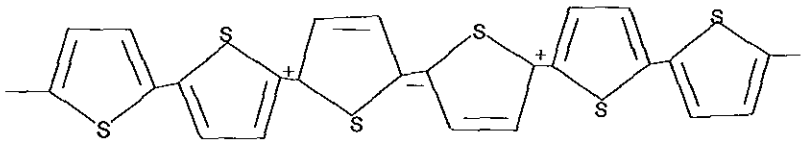

b)

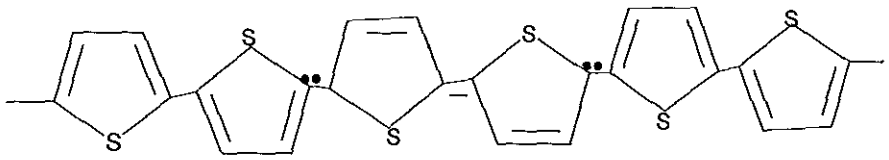

c)

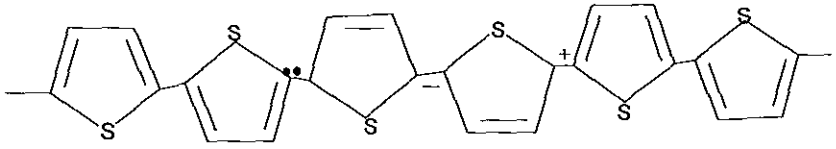

Fig.3.8 (a) Hole bipolaron, (b) Electron bipolaron (c) Exciton.

Polarons and bipolarons create two interacting states within the forbidden energy gap [36]. These two states are symmetric with respect to the gap center. The presence of new electronic states in the band gap makes new electronic transitions possible as shown in Fig. 3.9.

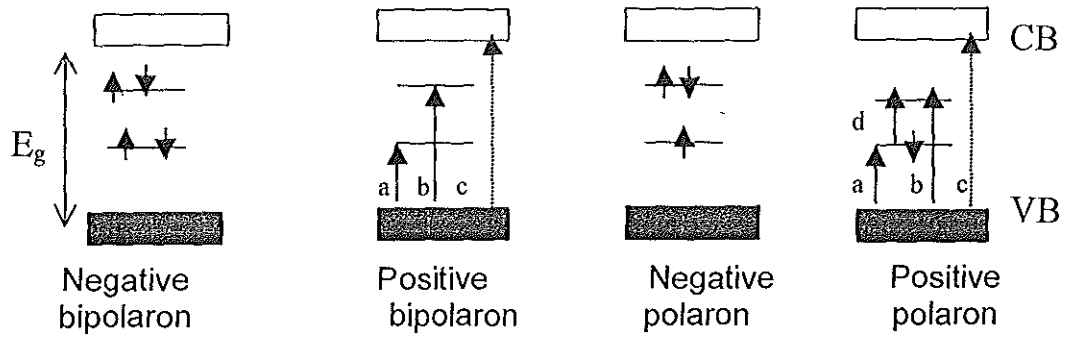


Fig.3.9.Energy band diagrams showing polaron and bipolaron states in the non-degenerate polymer. The arrows indicted by the letters a, b, c and d, represent the possible optical transitions.

When polymers are doped, two absorption features appear within the gap, corresponding to the new transitions as shown in the Fig.3.10 [37]. At higher level of doping polymers show metallic property [38].

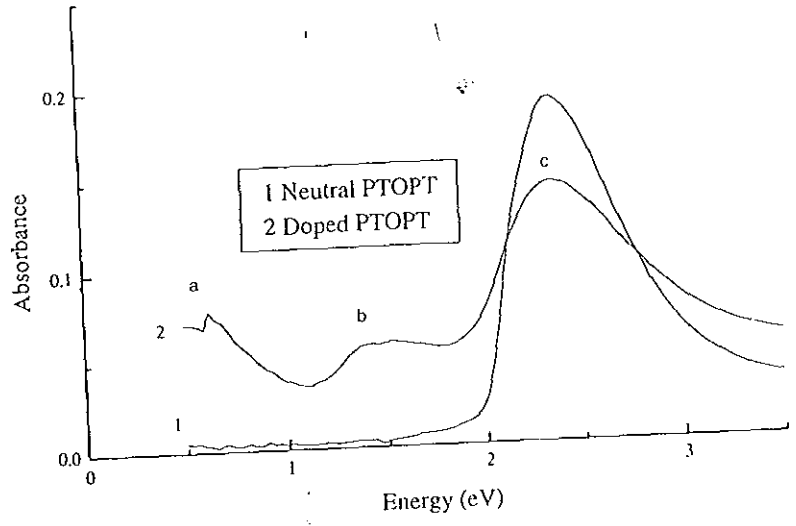


Fig. 3.10 Optical absorption spectra of (1) neutral and (2) doped PTOPT [37].

## 3.3 Charge Transport Mechanism

The prerequisite for charge transport is the presence of mobile charge carriers. The elementary equation of conductivity is

$$\sigma = ne\mu \qquad (3.1)$$

where, n is carrier concentration, e is elementary charge of the carriers and $\mu$ is mobility of the carriers.

In conducting polymers the conductivity is due to the presence of solitons, polarons and bipolarons, which are formed by self-localization of the carriers, introduced into the $\pi$ electronic systems through doping and in some cases during synthesis [39]. The characterization and modeling of electrical conductivity due to this charge carriers is difficult since conducting polymers are highly disordered with a considerable amount of impurities. The charge carriers are supposed to be mobile along the polymer chain. But actually, the carriers must hop not only across the defects in the conjugated system but also across the interchain and fibrillar gaps [40].

Conductivity of materials depends on temperature. Conductivity of metals increases when temperature decreases wile incase of inorganic semiconductors it decreases exponentially with decreasing temperature. For some metals, when temperature decreases, lattice vibrations, which act as obstacles for the charge carriers, freeze out. However, in case of crystalline semiconductors, both charge carriers and lattice vibrations freeze out.

In case of conjugated polymers conductivity depends on doping level. Park.et al identified three different regimes of doping to describe electrical conductivity in polyacetylene [41]. These are slightly doped, moderately doped and heavily doped. At low doping levels the temperature dependence of the conductivity is high. As the doping level increases, the dependence of the conductivity on temperature becomes less [42]. Because of these doping level dependence, the charge transport mechanism cannot be described by one single model over the whole range of doping level. Different models need to be applied to different regions.

In modeling the conductivity of polymers, hopping between localized defects and tunneling are often the dominant charge transport mechanisms. The value of the conductivity at zero temperature distinguishes tunneling and hopping conductivity. Hopping conductivity vanishes as temperature comes to zero but not tunneling [43].

Hopping conductivity is applicable for undoped and slightly doped polymers. In the undoped form, the electronic states responsible for charge transport in conjugated polymers are localized and have a very low mobility. The model suggested by Mott [44] called variable range hopping (VRH) best describes conductivity in conjugated polymers in their neutral states. Variable range hopping is a thermally activated transport near the Fermi level.

For polyacetylene, where solitons are dominant charge carriers, intersoliton hopping is the dominant conductivity mechanism. The solitons may be either neutral

or charged, see Fig. 3.11. The charged solitons are trapped by the dopant ions and neutral solitons are free to move. When neutral soliton passes close by a charged soliton, an electron can hop between the mid gap states belonging to the solitons [45]

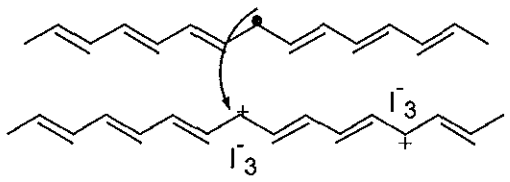


Fig.3.11. Intersoliton hopping in *trans*- polyacetylene [22].

Electrons hop from occupied states to empty states with the assistance of phonons. These phonons are available at high temperature and freeze out at very low temperature. The temperature dependence of hopping conductivity is given by [44]

$$\sigma = \sigma_0 \exp[-(T_0/T)^{\gamma}] \qquad (3.2)$$

where $\gamma$ depends on dimensionality d of the hopping process as

$$\gamma = \frac{1}{1+d}$$

$\gamma$ equals 1/4,1/3 and 1/2, which corresponds to hopping in three, two and one dimensions, respectively. This model is used at low bias, since conductivity is

dependent on electric field that affects the dimensionality d [46]. Considering inter-chain hopping, i.e., three-dimensional conductivity, $\gamma$ = 1/4, which results in Mott's famous "$T^{-1/4}$ " low.

$$\sigma = \sigma_0 \exp[-(T_0/T)^{1/4}] \qquad (3.3)$$

with $\sigma_0 = e^2 N(E_F)\, d\nu_{ph}$, Where d is the average hopping distance,

$$d = [8/9\pi\alpha N(E_F)\, kT]^{-\gamma}$$

$$T_0 = 8^3\alpha^3/9\pi k N(E_F)$$

$\alpha$ inverse localization length, $\nu_{ph}$ is typical phonon frequency and $N(E_F)$ is density of states given by

$$N(E_F) = \frac{\nu}{(2\pi)^3} \int \frac{ds_E}{v_g}$$

where $v_g$ is group velocity.

When doping level increases, a model with small conducting islands with metallic conductivity separated by insulating barriers is used. These barriers have been suggested to be conjugational defects, segments of undoped or weakly doped polymer chains, interchain or fibrillar contacts or other inhomogenities [46-48]. In such a case tunneling conductivity becomes dominant. Depending on the size of the insulating barriers, the temperature dependence of tunneling conductivity has been given by (when the size of the barrier is sufficiently small)

$$\sigma = \sigma_0 \exp[-(T_0/T)^{1/2}] \quad (3.4)$$

where $\sigma_0$, $T_0$ as specified in hoping conductivity. When the size of the barrier height is larger, then

$$\sigma = \sigma_1 \exp[-T_1/(T_2+T)] \quad (3.5)$$

where $T_1$ and $T_2$ are material constants dependent on the width and height of the tunneling barrier.

## 4. Metal-Semiconductor Contact

When two different conducting materials come into intimate contact, the energy band edges near the interface will be discontinued. This is due to the fact that materials generally do not have the same energy band gap. That is the position of the Fermi-levels of the two materials is different before contact is made. When contact is made, there will be a net charge at the surface that causes an electric field. This electric field produced in the semiconductor causes the flow of charge carriers from the semiconductor to the metal or vice versa and consequently bending of the band comes about. The motion of charge carriers from the semiconductor to the metal creates depleted region with depletion width W [49]. In Fig.4.1, we have illustrated a band diagram of a metal and an n-type semiconductor with work functions $\phi_m$ and $\phi_s$, respectively, where $\phi_m > \phi_s$. As shown in the figure, relative to the fermi level of the metal, the fermi level of the semiconductor is lowered by an amount equal to the difference between the two work functions.

This bending of the band edge and creation of barrier height is an important feature for all semiconductor devices. The barrier height is nothing but the difference between the work function of the metal and electron affinity of the semiconductor. Work function of the metal is the amount of energy required to remove an electron from the fermi-level to a state of rest, that is, vacuum level. The electron affinity of a semiconductor is the difference in energy between an

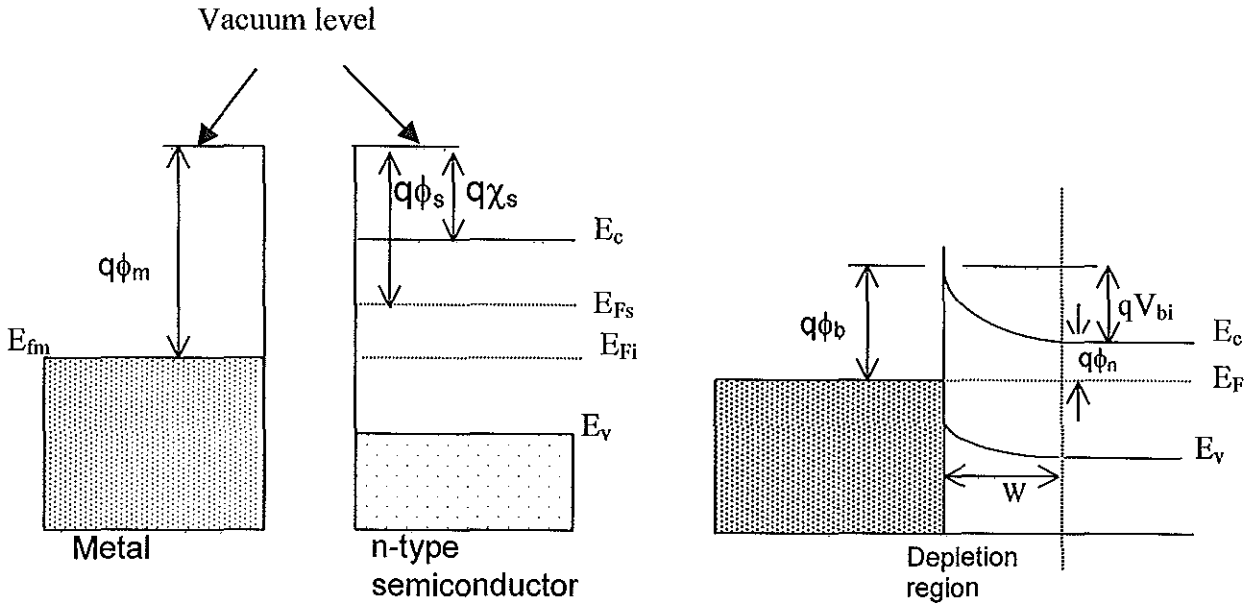


Fig.4.1. Energy band diagram of a metal and n-type semiconductor ($\phi_m > \phi_s$) a) before, b) after contact.

electron located at the vacuum level and an electron at the bottom of the conduction band [50].

$$\phi_b = \phi_m - \chi_s \qquad (4.1)$$

where $\phi_m$ is work function of the metal and $\chi_s$ is electron affinity of the semiconductor. On the semiconductor side there is a parameter called the built in potential ($V_{bi}$) which is given by [51]

$$V_{bi} = \phi_b - \phi_n \tag{4.2}$$

Considering the contact of a low work function metal and p-type semiconductor, the band will bend as shown in Fig.4.2. For an ideal contact between the metal and p-type semiconductor, the barrier height is given by [51]

$$\phi_b = E_g - (\phi_m - \chi_s) \tag{4.3}$$

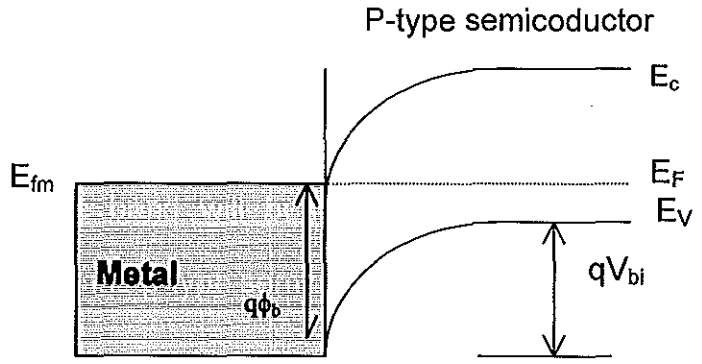


Fig.4.2 Energy band diagram of a metal and p-type semiconductor ($\phi_m<\phi_s$) at equilibrium.

If a positive voltage is applied to the semiconductor with respect to the metal, the built-in potential will be reduced to $V_{bi} - V_F$ (we use the subscript F to indicate that the junction is forward biased when the semiconductor is connected to the positive polarity of the voltage source). But the barrier height in the side of the metal

remains the same. This makes easier for the holes to flow from the semiconductor to the metal, see Fig.4.3. On the other hand if we apply negative voltage to the semiconductor, which is the reverse bias condition, the barrier in the side of the semiconductor increases to $V_{bi}$ +$V_F$. This makes the flow of carriers to the metal difficult [50].

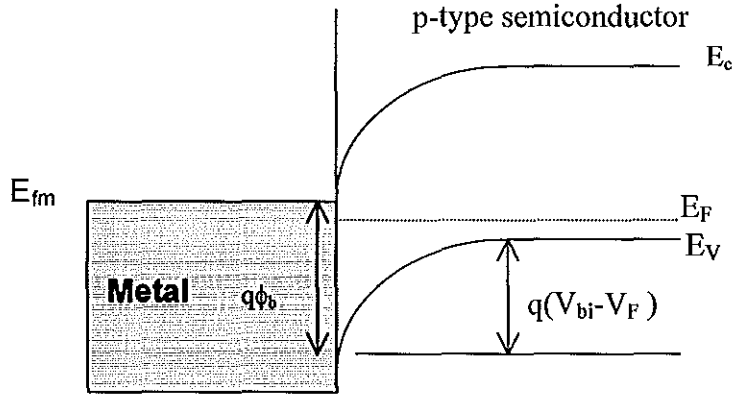


Fig.4.3. Band diagram for metal and p-type semiconductor when forward bias voltage ($V_F$) is applied.

## 4.1. Charge Transport Mechanism Across the Junction

Drift or diffusion causes transport of charge carriers (current) in conducting materials. Drift is due to applied electric field, where as diffusion is due to difference in carrier concentration.

The four basic process that occur under a forward bias are a) emission of the carriers over the top of the barrier, b) quantum mechanical tunneling through the barrier, c) recombination in the space charge region, d) recombination in the neutral region [51] as shown in Fig. 4.4.

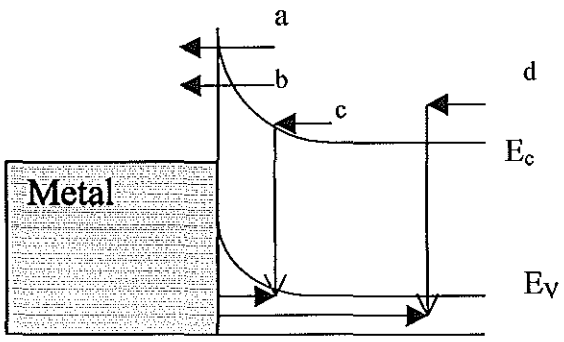


Fig.4.4.The four basic transport mechanisms of a Schottky diode under forward bias of a metal and n-type semiconductor junction.

*Emission over the barrier:* The current flow across the barrier is due to carrier transport from the edge of the space charge layer to the metal. When we apply a forward bias, carriers move through the depletion layer and emitted from the semiconductor to the metal by going over the barrier as shown by arrow (a) in Fig.4.4.

*Tunneling Current*: When the semiconductor has a high concentration of charge carriers, tunneling through the barrier occur due to the reduction of depletion width.

This flow of charge carriers through the barrier has equal probability for each direction at equilibrium condition. It is indicated by arrow (b) in the above figure.

*Recombination current*: When we apply a forward bias, it increases the charge carrier concentration at the edge of the space charge layer. These excess carriers may cross the space charge layer so that the carrier concentration exceeds the equilibrium values. Consequently recombination occurs as indicated by arrow (c).

*Hole injection:* If the height of the Sckottky barrier on n-type semiconductor is greater than half of the band gap then the region of the semiconductor adjacent to the metal contains a high density of holes. These holes may diffuse in to the neutral region of the semiconductor under forward bias, which results injection of holes see Fig. 4.4 arrow (d).

The current in a Schottky barrier diode is interpreted using thermionic emission theory [49]. In thermionic emission theory, not all charge carriers cross the junction barrier, but only those carriers that have a velocity component normal to the interface, and an energy greater than $E_f + q\phi_m$ are capable of crossing [48]. The familiar current density equation obtained from the thermionic emission theory is given by[50]

$$J = J_0\left[\exp\left(\frac{qV}{nkT}\right) - 1\right] \qquad (4.4)$$

where J is current density at an applied voltage V, $J_0$ is reverse saturation current density, q is the charge of an electron, k is the boltzmann constant, T is absolute temperature and n is the diode quality factor. The reverse saturation current is given by

$$J_0 = A^* T^2 \exp\left(\frac{-q\phi_b}{kT}\right) \qquad (4.5)$$

where $A^*$ is the modified Richardson constant, $\phi_b$ is barrier height.

There are three possible current-voltage (I-V) characteristics depending on the relative magnitudes of J and $J_0$. These are

I) If $J >> J_0$ the contact will completely block current flow in the reverse direction and allows current in the forward direction. Then eq. 4.3 is applicable to the rectifying diode.

II) If $J << J_0$, the equation can be expanded and a linear relation of J-V will be obtained

$$V = \left(\frac{nkT}{J_0 q}\right) J$$

which is Ohms low

III) If $J = J_0$, the contact will be neither ohmic nor rectifying.

If the junction obeys the first condition, we can find $J_0$ by extrapolating the linear part of lnJ–V plot to the lnJ-axis at small forward bias voltage. After determining $J_0$ , we can determine the barrier height from the relation

$$\phi_b = \frac{kT}{q} \ln\left(\frac{A^* T^2}{J_0}\right) \qquad (4.6)$$

where $A^*$ is equal to $120 Ak^2/cm^2$, and the ideality factor(n) of the diode can be calculated from the relation

$$n = \frac{q}{kT\left(\frac{\partial \ln J}{\partial V}\right)} \qquad (4.7)$$

For ideal diodes, the diode quality factor n = 1. All real diodes have n >1. If trapping and recombination of charge carriers is high, then $n \geq 2$ [49].

## 4.2 Impedance Spectroscopy and Circuit Models

It is one of the techniques used to study the properties of junctions formed by any two electronically conducting materials. From this technique we can find the resistance(R) and capacitance (C), of the junction. Impedance is measured in the

frequency domain by applying voltage or current to the device under test and measuring the resulting current or voltage. The impedance is expressed as a complex number:

$$Z = Z_r + jZ_i \qquad (4.8)$$

where, $j = \sqrt{-1}$ and $Z_r$ and $Z_i$ are the real and imaginary parts of the impedance, respectively.

The real and imaginary parts of the impedance are recorded as a function of frequency and plotted in a complex plane. The real part is plotted along the x-axis and the negative of the imaginary along the y-axis. Ideally the imaginary part of the impedance is zero at frequencies, $\omega$=0 and $\omega$ approach to $\infty$[52]. This plot forms a semicircle with the center on the real axis.

One of the most important advantages of impedance spectroscopy is direct correlation between the response of a real system and an idealized model circuit composed of discrete electrical components. For the interface formed by metal-polymer contacts, the resistance(R) represents the dissipative component and the capacitance(C) describes the storage component. These resistances and capacitances can be combined in different forms according to the nature of the interface formed. We shall begin by taking a simple parallel R-C circuit as shown in Fig.4.6 [53]. The impedance of this model is given by

$$Z = \frac{R}{1 + j\omega RC}$$

Normalizing this

$$Z = \frac{R - jR^2\omega C}{1 + \omega^2 R^2 C^2}, \text{ then } Z_r = \frac{R}{1 + \omega^2 R^2 C^2} \text{ and } Z_i = \frac{-R^2\omega C}{1 + \omega^2 R^2 C^2}$$

a) b)

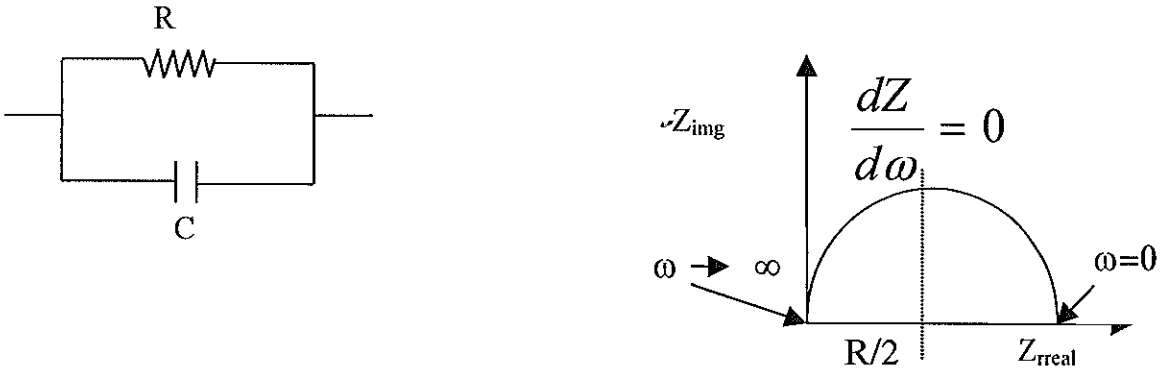


Fig.4.5. Circuit model (a) and idealized Cole-Cole plot of $-Z_{img}$ versus $Z_{real}$ as a function of frequency scanned from 0 to ∞ (b) for M-S contact [52]. r is radius.

By evaluating $dZ_i/d\omega = 0$ we can get the value of the resistance as a function of $Z_{imax}$. In doing this, $R = 2(-Z_{imax})$. If there is a contact resistance in series with the RC parallel circuit, the impedance will be

$$Z = R_c + \frac{R}{1 + j\omega RC}$$

whose circuit (a) and Cole-Cole plot (b) is illustrated below in fig.4.8

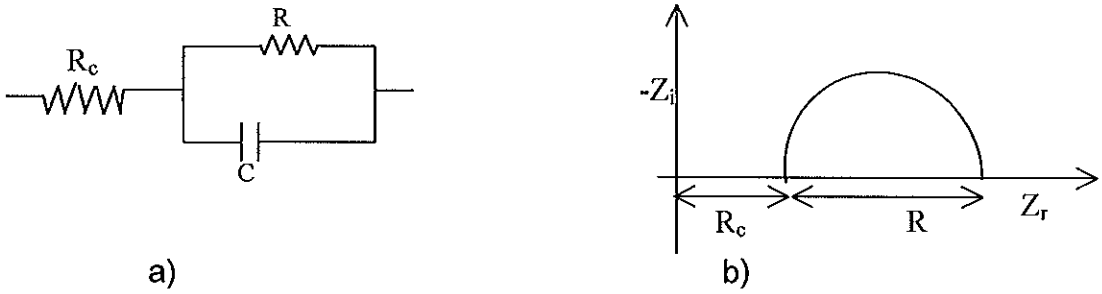


Fig.4.6. Circuit for M-S contact in series with contact resistance $R_c$ (a) and the corresponding idealized Cole-Cole plot (b).

For a metal-insulator-semiconductor device, the model consists two resistors ($R_1$ and $R_2$) and two capacitors ($C_1$ and $C_2$) where $R_1$ and $C_1$ represent the insulating layer, while $R_2$ and $C_2$ stand for the depletion region. The corresponding impedance will be

$$Z = R_c + \frac{R_1}{1 + j\omega R_1 C_1} + \frac{R_2}{1 + j\omega R_2 C_2}$$

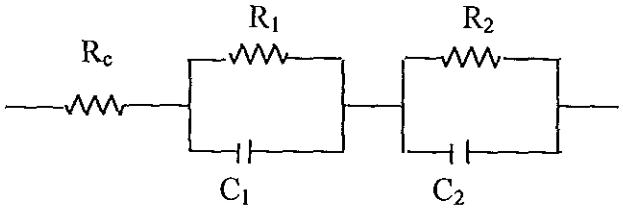


Figure 4.7. Circuit model for M-I-S junction.

The complex impedance plot of such a device consists of two semicircles as shown in Fig.4.8.

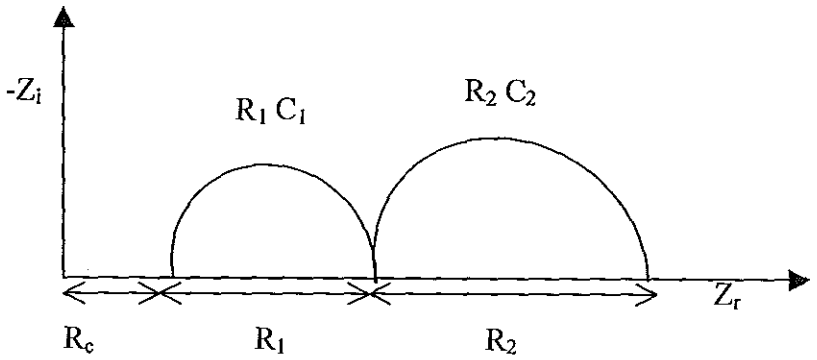


Figure 4.8. An idealized Cole-Cole Plot for the circuit shown in fig. 4.7.

# 5. Experimental

## 5.1 Sample preparation

Commercially available transparent conductor on glass called indium tinoxide, ITO/glass substrate was cut out in an appropriate size and washed with distilled water, ethanol, and rinsed with acetone. These cleaned pieces were partly covered by photoresist. The exposed part of the ITO was etched out with a mixture of hydrochloric acid, sulfuric acid and water with a ratio of 48: 4: 48 by volume, respectively as shown in Fig 5.1(a). Then the photoresist was removed using acetone and then thoroughly cleaned.

Two different types of diodes with PDOPT as an active organic semiconductor were prepared for characterization. For both types of diodes, a chloroform solution of PDOPT with a concentration of 4mg/ml was prepared and kept in a clean and cool place. The first type of the devices was made by spin coating PDOPT solution on the ITO/glass substrate, while the second type was made such that a commercially available liquid PEDOT-PSS was spin coated on ITO/glass followed by spin coating of PDOPT on top. All spin coating process were done using a programmable spinner system at a speed of 600 rpm which yielded a thin (about 100nm) uniform films. On both types of diodes, aluminum (as a low work function metal) was evaporated at a pressure of about $2\times10^{-6}$ mbr to form Al/PDOPT/ITO and Al/PDOPT/PEDOT-PSS/ITO sandwich strictures, respectively,

as shown in Fig. 5.1 (b, c). The commercially available PEDOT-PSS is a relatively highly conducting polymer complex. It is used in the second type diode merely to enhance charge transport. The active area of the diodes was about $3\times10^{-2}$ $cm^2$.

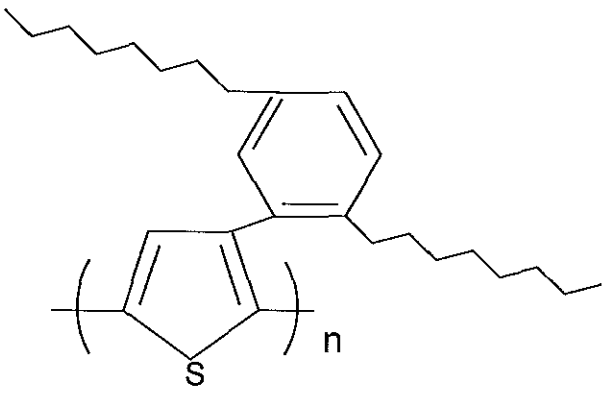


a)

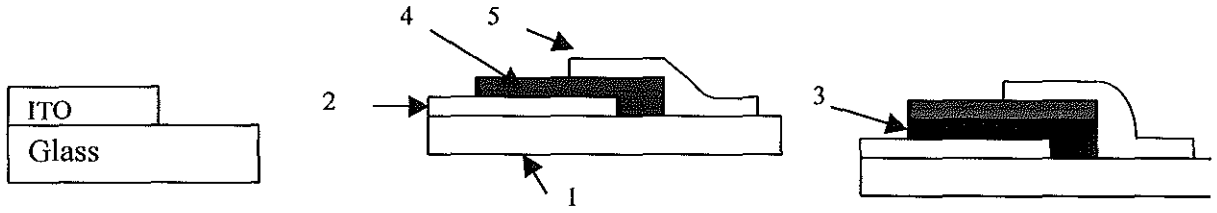


(b) (c) d)

Fig.5.1 (a) chemical stracture of PDOPT, (b) substrate prepared for the deposition of polymer, (c and d) the working samples Al/PDOPT/ITO and Al/PDOPT/PEDOT-PSS/ITO, respectively. The numbers 1,2,3,4 and 5 represent Glass, ITO, PEDOT-PSS, PDOPT and Al, respectively.

## 5.2 Current-Voltage Measurement

The current density-voltage characteristics of the diodes were measured by using HP 4140B pA Meter/DC Voltage Source, together with HP 16055A-test fixture. During the measurement, the samples were placed at room temperature, dry air and in the dark. The applied voltage was scanned between -2.5V to +2.5V. In this measurement the data were taken point by point with two-minute interval and a step voltage of 0.1V. The plots of J-V and lnJ-V curves are shown in fig. 6.1 and fig. 6.2 respectively.

## 5.3 Impedance Measurement

Complex impedance spectroscopy of the diodes was measured as a function of frequency and applied bias voltage using an HP 4192A LF Impedance Analyzer together with an HP 16047A-test fixture. The Cole-Cole plots for Al/PDOPT/PEDOPT-PSS/ITO and Al/PDOPT/ITO structures are shawn in Fig. 6.4, 6.5 and 6.6. The data were taken in frequency range between 0.5kHz to 100k Hz for bias voltages ±3v, ±2v, and ±1v. For every applied bias voltage a sinusoidally oscillating voltage of $V_{rms}$ =10mV was used.

# 6. Results and Discussions

## 6.1. Current-Voltage Characteristics

Figure 6.1 shows the J-V characteristics of Al/PDOPT/PEDOT-PSS/ITO (a) and Al/PDOPT/ITO (b) diodes in the dark at room temperature. Under forward bias, which corresponds to positives voltages applied to ITO electrodes, the current increased fast, where as in the reverse direction the current was almost blocked. This confirms the formation of a Schottky barrier type at the interface between aluminum and the polymer. According to the theory of Schottky barrier, the work function of the metal must be smaller than that of the p-type semiconductor and a rectifying barrier would be formed at the interface. If the work functions were in reverse order, an ohmic contact would be created rather than rectifying. The interface between aluminum and polymer is rectifying and between polymer and ITO is ohmic. So the polymer, PDOPT, is a p-type semiconductor whose work function is between that of aluminum and ITO as observed from the rectification characterstics of the diodes.

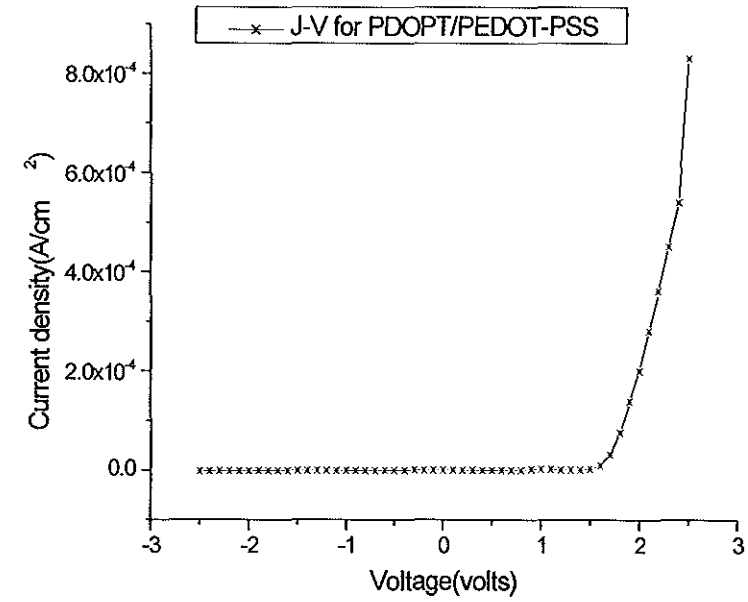


a)

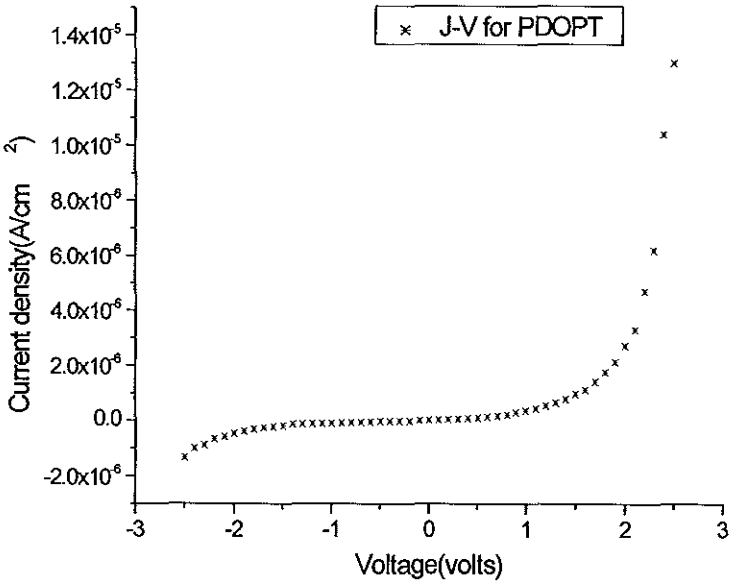


b)

Figure 6.1. Current density versus applied voltage at room temperature of Al/PDOPT/PEDOT-PSS/ITO (a) and Al/PDOPT/ITO (b) diodes.

Depending on the applied voltage in the forward direction, a semilogaritmic plot (fig. 6.2) of the forward current density (J) versus the applied voltage (V) shows three types of regions. In the voltage range, 0<V<1.3 for Al/PDOPT/PEDOT-PSS/ITO diode, the current increase slowly. This may be due to recombination of electrons and holes in the depletion region. Between the voltages 1.3V and 1.9V, the currents grow faster and form a straight line, showing formation of depletion layer between aluminum and the polymer. In this region qV/kT >> 1, so that we can use the modified Schotky diode equation.

$$J = J_0 \exp\left(\frac{qV}{nkT}\right)$$

When the applied voltage increase further beyond 1.9V, the bulk resistance of the polymer limits the current.

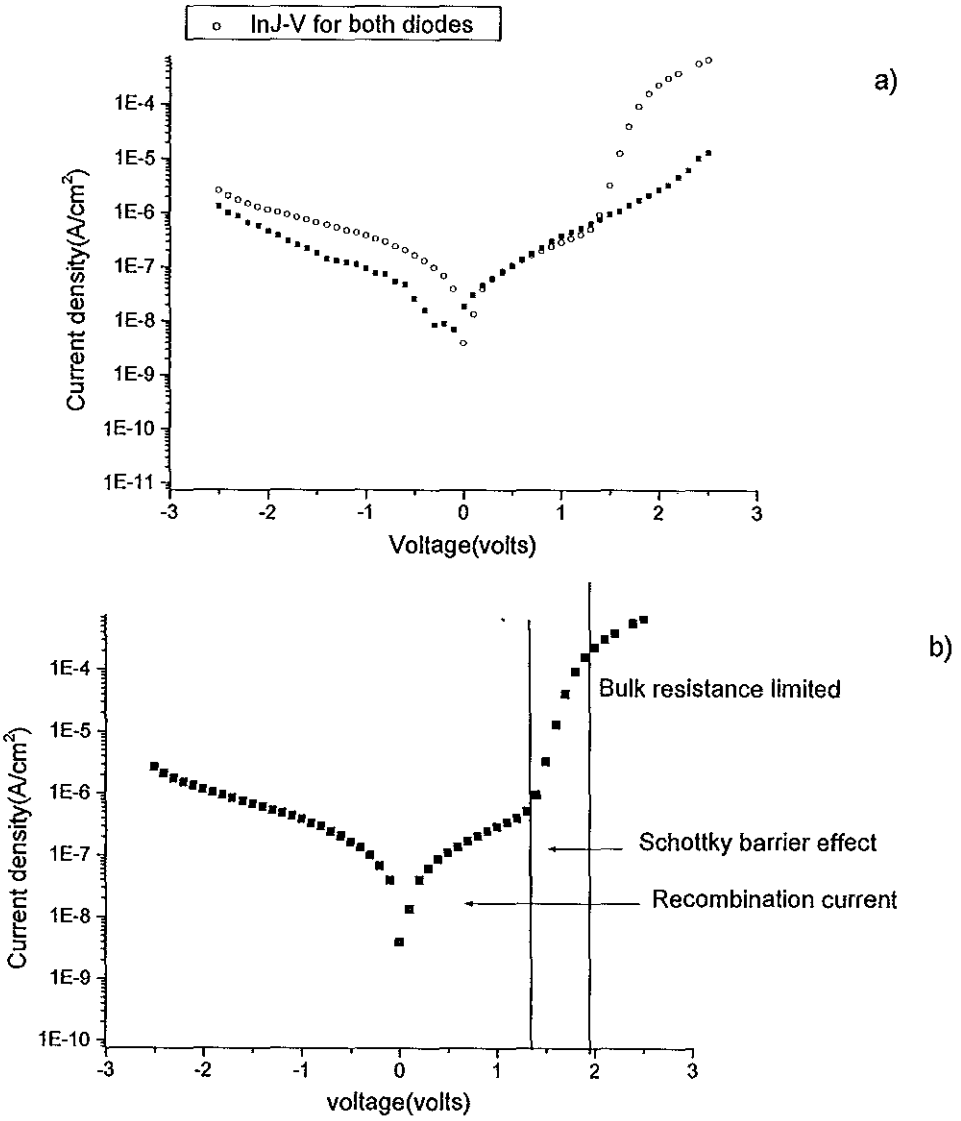


Fig.6.2. The logarithm of current density vs. voltage for a) Al/PDOPT/PEDOT-PSS/ITO (open circles) and Al/PDOPT/ITO (solid squares), b) InJ-V for Al/PDOPT/PEDOT-PSS/ITO diode showing the three regions in the forward bias.

The forward current increases exponentially in the voltage range 1.3V to 1.9V. As a result, these devices clearly exhibit rectifying behavior in the dark, with a rectification ratio of 330 and 10 at ±2.5V for Al/PDOPT/PEDOT-PSS/ITO and Al/PDOPT/ITO diodes, respectively.

By extrapolating the straight line to zero voltage, the reverse saturation current densities $J_0$ are obtained to be $6\times10^{-12}$ A/cm$^2$ and $7\times10^{-11}$A/cm$^2$ for Al/PDOPT/PEDOT-PSS/ITO and Al/PDOPT/ITO, respectively (Table 6.1). And the barrier height of Al/PDOPT calculated using equation 4.6 is 1.1eV in case of Al/PDOPT/PEDOT-PSS/ITO diode and 1eV for Al/PDOPT/ITO diode. By using equation 4.3, the electron affinity of the polymer is 3.3ev using $\phi_b$ of Al/PDOPT/PEDOT-PSS/ITO diode. The ideality factor of 1.5 and 2.3 were obtained for the Al/PDOPT/PEDOT-PSS/ITO and Al/PDOPT/ITO, respectively.

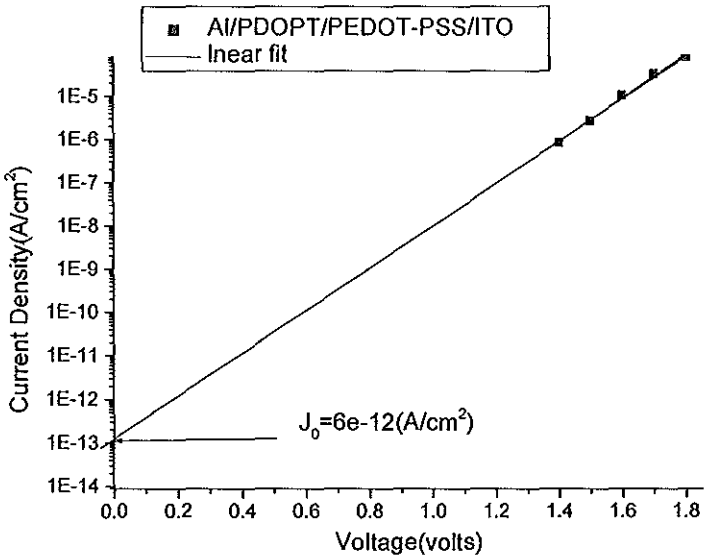


Fig.6.3. Linear part of lnJ versus V curve for Al/PDOPT/PEDOT-PSS/ITO diode.

The rectification and ideality factors are different for Al/PDOPT/PEDOT-PSS/ITO and Al/PDOPT/ITO diodes. This is due to the fact that PEDOT-PSS has relatively higher conductivity and the interface between PDOPT and PEDOT-PSS is conducive for charge transfer as the result of the interpenetrating nature of the polymers [11]. Moreover, the presence of PEDOT-PSS layer increases the conductivity because the injection/collection properties of the PEDOT-PSS/PDOPT interface are superior to those of the ITO/PDOPT interface.

Table 6.1. Parameters extracted from the current-voltage characteristics of Al/PDOPT/PEDOT-PSS/ITO and Al/PDOPT/ITO (primed) sandwich structures of Fig. 6.2.

| $J_0'(A/cm^2)$ | $J_0(A/cm^2)$ | $\Phi_b'(eV)$ | $\phi_b(eV)$ | n' | n | $\gamma'$ | $\gamma$ |
|---|---|---|---|---|---|---|---|
| $7\times10^{-11}$ | $6\times10^{-12}$ | 1 | 1.1 | 2.3 | 1.5 | 10 | 330 |

## 6.2 Complex Impedance Analysis

Figure 6.6 shows the complex impedance spectroscopy of Schottky diodes made of Al/PDOPT/ITO and Al/PDOPT/PEDOT-PSS/ITO sandwich structures as a function of frequency and bias voltages. During this measurement a sinusoidal oscillating voltage of $V_{rms}$=10mV is added for each bias voltages. The frequency ranges from 0.5kHz to 100kHz. The filled points are the measured coordinates of the real and imaginary parts of the impedance.

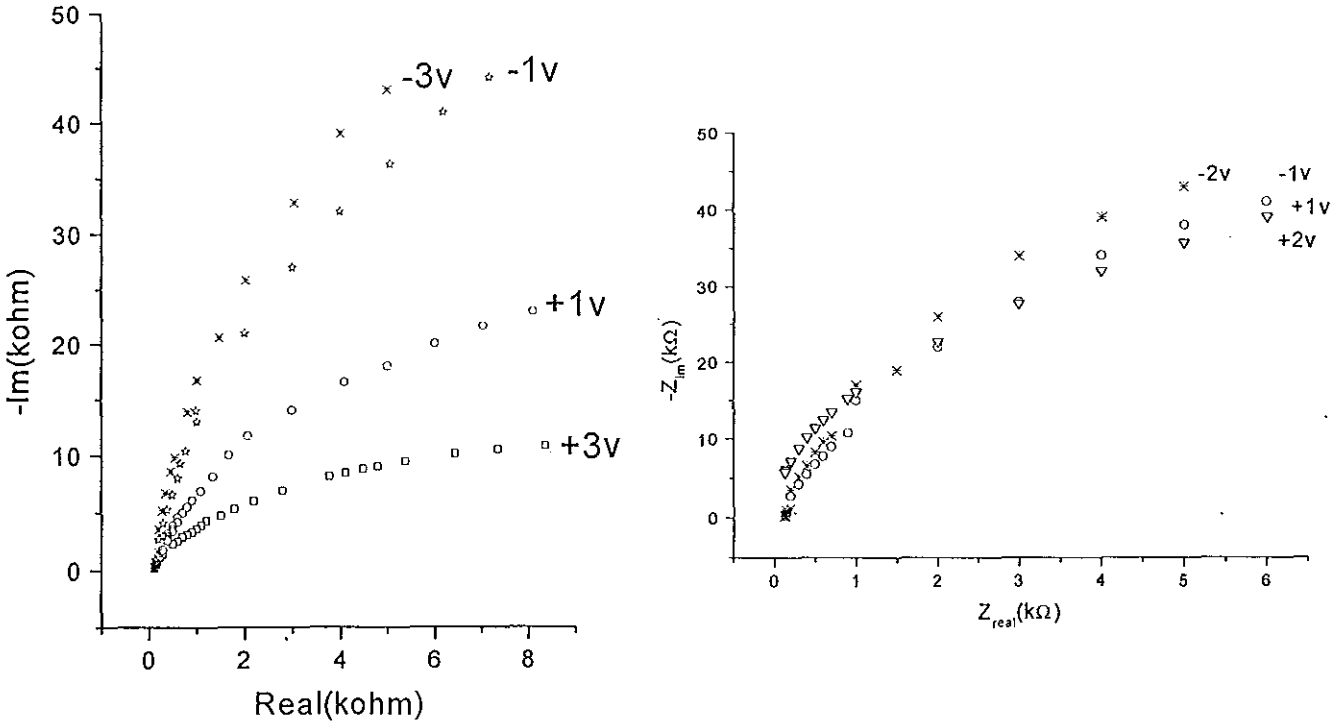


a) b)

Fig. 6.4 Cole-Cole plots of (a) Al/PDOPT/PEDOT-PSS/ITO and (b)Al/PDOPT/ITO sandwich structures.

The plot of $-Z_{imaginary}$ vs. $Z_{real}$ consists of parts of semicircles whose diameters are bias voltage dependant. Since an R-C parallel circuit yields a semicircle in the complex plane, we can model our diode (Al/PDOPT/ITO) by a one parallel R-C circuit in series with the contact resistance, $R_c$. The diameter of the extrapolated semicircle represented by $Z_{real}$ is the resistance of the depletion region. To find this resistance (R), a circular fit to the complex impedance representation was performed with the help of origin. The capacitance was estimated from the relation $(-Z_{im}) = (C\omega)^{-1}$ at highest value of $Z_{im}$, knowing the value of $\omega$ for which $Z_{img}$ was maximum.

The Cole-Cole plots of the impedance measurements are consistent with our current voltage curves (Fig 6.1). For the bilayer sample, resistance is very large at reverse bias voltages and small at forward bias, which is consistent with its rectification property. From the Cole-Cole plot Fig 6.6, two partially overlapping semicircles are observed at –1V and –3V bias voltages. This shows the formation of thin insulating layer at the aluminum polymer interface [54]. The left (high frequency) small semicircle represents the thin insulating layer and the (right) larger low frequency semicircle represents the depletion region, which is strongly dependent on bias voltage. The structure may be interpreted as a metal-Insulator-Semiconductor (MS'S) junction whose circuit model illustrated in Fig 4.7. The fact that no two distinct semicircles observed at +1V and +3V bias voltages is due to the reduction of the depletion region thereby resulting in total overlapping of the two semicircles.

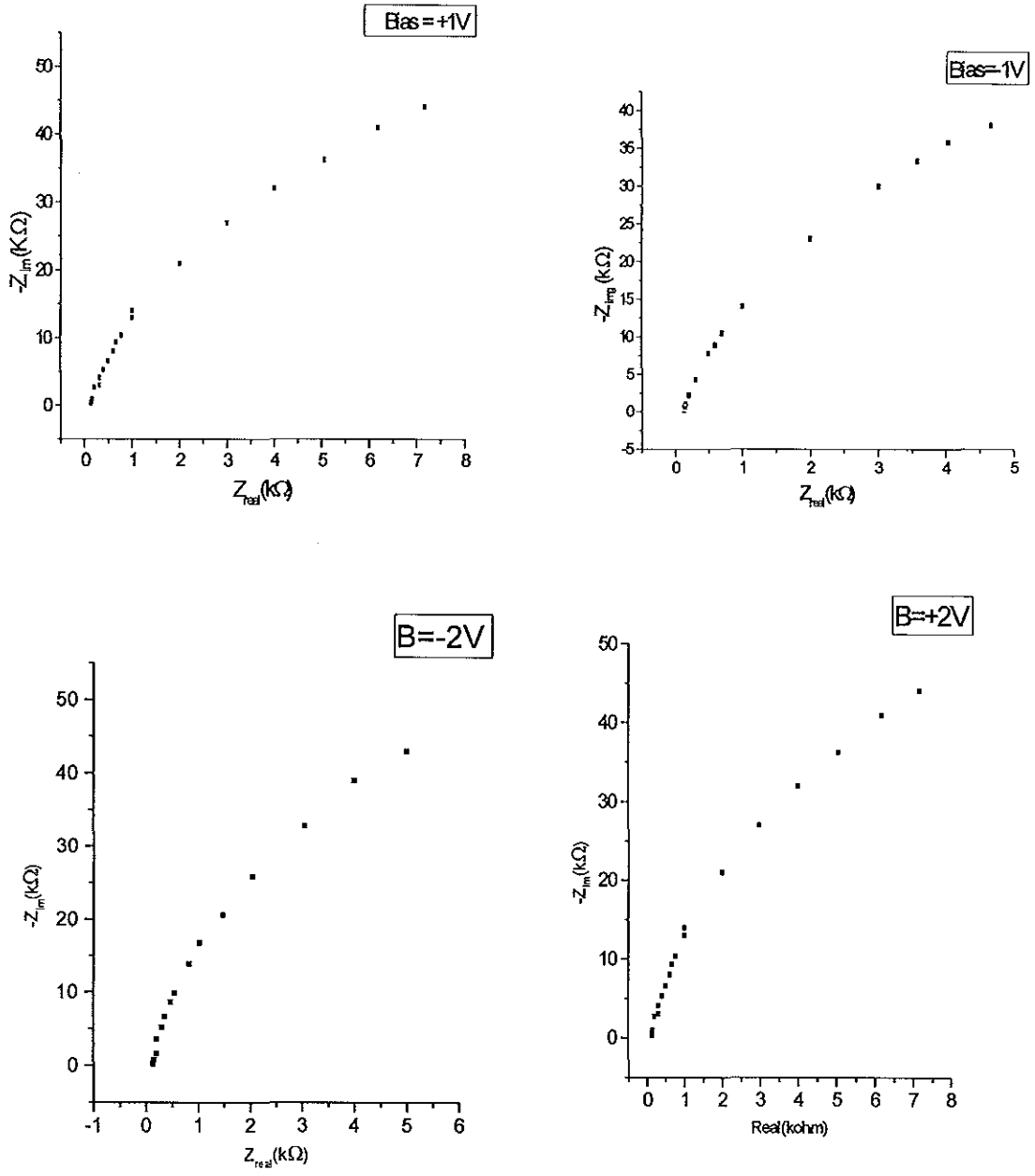


Fig.6.5. The Cole- Cole plots of Al/PDOPT/ITO diodes at different bias voltages.

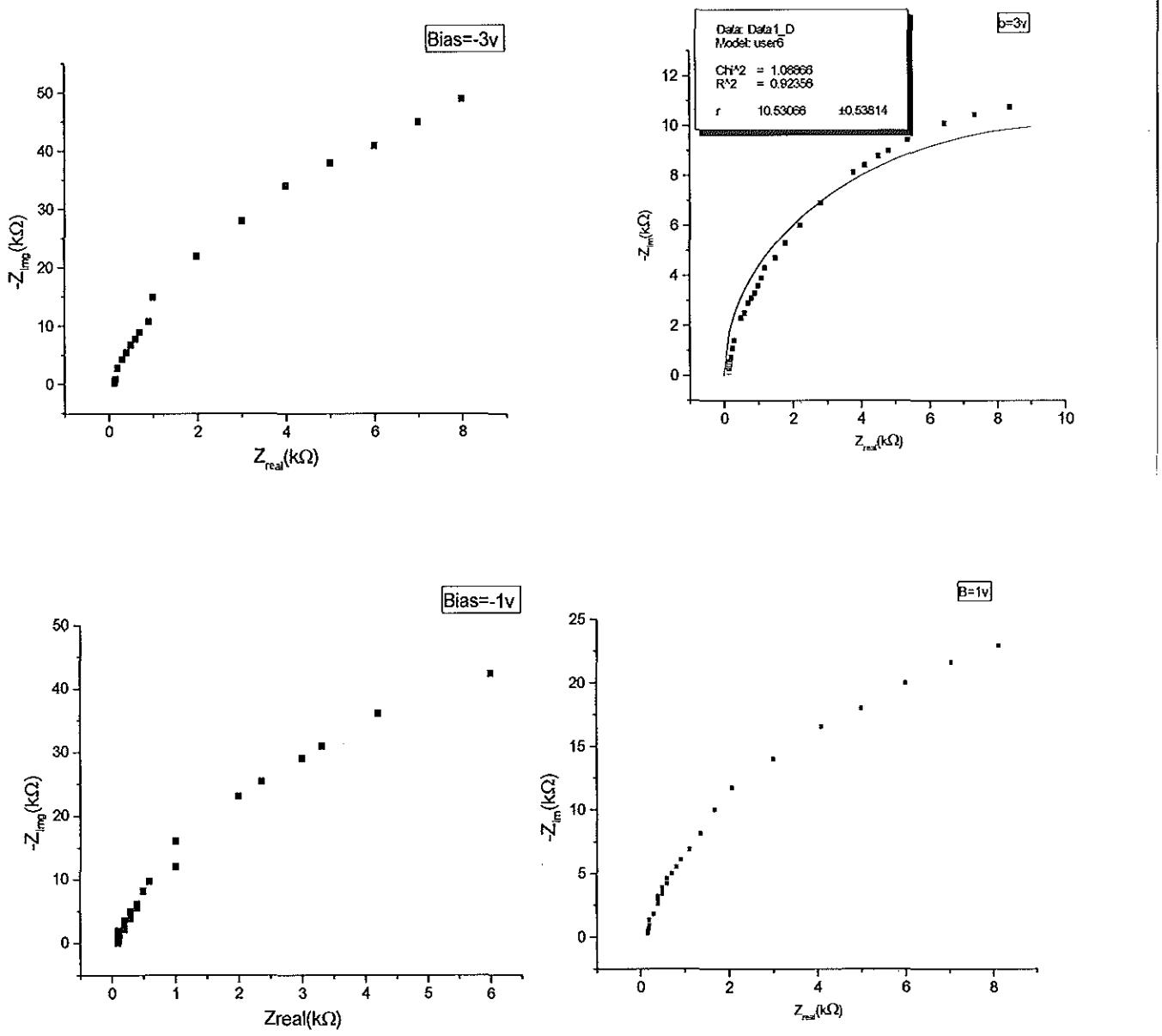


Fig. 6.6 Cole-Cole plots of Al/PDOPT /PEDOT -PSS/ITO diode.

From Fig. 6.5 and 6.6 the complex impedance spectra show that presence of PEDOT-PSS layer enhances conductivity owing to high injection/collection property at PEDOT-PSS/PDOPT interface. The ranges of the resistances in reverse and forward bias voltages confirm with the rectification of the two diodes. The parameters obtained from fig. 6.5 and 6.6 are listed in Tables 6.2 and 6.3, respectively.

Table 6.2. Parameters obtained from the Cole-Cole plots of Al/PDOPT /ITO diode fig 6.5. $V_b$-bias voltage, $R_c$ –contact resistance, $R_d$-depletion layer resistance and $C_d$-capacitance of the depletion region. The negative values of the voltage correspond to the reverse bias.

| $V_b$ (volts) | $R_c$ (Ω) | $R_d$ (kΩ) | $C_d(10^{-9}$ F/cm$^2$) |
|---|---|---|---|
| -2 | 130 | 292 | 57 |
| -1 | 130 | 260 | 67 |
| 1 | 130 | 244 | 83 |
| 2 | 120 | 226 | 96 |

Table 6.3 Parameters extracted from the Cole-Cole plots of Al/PDOPT/PEDOT-PSS/ITO sandwich structure fig 6.6. $R_s$ and $C_s$ are resistance and capacitance of the insulating layer.

| $V_b$(voltes) | $R_c(\Omega)$ | $R_d(k\Omega)$ | $C_d(10^{-9}F/cm^2)$ | $R_s(k\Omega)$ | $C_s(10^{-9}F/cm^2)$ |
|---|---|---|---|---|---|
| -3 | 150 | 258 | 34 | 100 | 26 |
| -1 | 130 | 202 | 37 | 120 | 23 |
| +1 | 150 | 56 | 37 | | |
| +3 | 130 | 21 | 44 | | |

## Conclusion

We have prepared diodes Al/PDOPT/PEOPT-PSS/ITO and Al/PDOPT/ITO sandwich structures, in which PDOPT is an active component. The J-V characteristics were studied using thermionic emission theory. The J-V characteristics of the two diodes show rectification. The bilayer diode is found to be more rectifying than the single layer devices. Use of PEDOT-PSS greatly enhances the diode quality. The ideality factor of a single layer diode is large due to trapping and recombination.

Single layer, thick film Al/PDOPT/ITO diode [20] was found to give non-linear non-rectifying I-V curves. However, if the film of PDOPT is made thin enough by spin coating, the diode rectifies. This is because the bulk resistance of thick films dominates the Schottky behavior of the junction. Introducing a conductive PEDOT-PSS polymer complex over the ITO/glass reduces the recombination and trap which is manifested in the value of the diode quality factor (n=1.5), and the rectification ratio of 330. It is there fore highly recommended that a thin layer of PEDOT-PSS be spin coated over ITO/glass substrate inorder to enhance the electron/hole injection. It is observed from our studies that using bilayer diode increases the rectification ratio by a factor of 33, and changes the non-ideality factor from 2.3 to 1.5. Further use of PEDOT-PSS thin film would make the bilayer diode a candidate of solar cells. Thus it will be the task of future investigations of photovoltaic property of

Al/PDOPT/PEDOT-PSS/ITO diodes as it is seen from Table 6.1 that this device has $J_0 = 6 \times 10^{-12}$ A/cm$^2$ and n = 1.5 which are indicators of photovoltaic properties.

The Cole-Cole plots of both types of diodes are consistent with their rectification behavior. However, the single layer diodes and the bilayer diodes at forward bias voltage manifest part of a single semicircle plot on a complex impedance plane. It is possible to model such diodes showing the feature of a parallel R C circuit. This is typical of metal-semiconductor junction property. On the other hand, the Al/PDOPT/PEDOT-PSS/ITO diodes manifest parts of two partially overlapping semicircles upon the application of reverse bias voltages. This may be attributed due to the relatively thicker film of the bilayer, which gives rise to higher value of the bulk resistance. The complex impedance of such a system senses as if there are two distinct regions with regards to resistance, one the common depletion region and the other due to a highly resistive nature of polystyrene sulphonate (PSS) in PEDOT-PSS. This component dangles out of the random coil when a reverse bias is applied as a result of which a resistive layer is formed at the interface. Such a behavior may be modeled as metal-insulator-semiconductor junctions. Its electrical circuit may be interpreted as two parallel RC connected in series.

## References


1. H. Shirakawa, E.J. Louis, A. G. MacDiarmid, C. K. Chiang, and A. J. Heeger, *J. Chem. Com.,* **16** (1977) 578.
2. L. H. Sperling, *Introduction to Physical Polymer Science*, John Wiley & Sons, Inc., New York, (1986).
3. J. Kaniki, *Handbook of Conducting Polymers*, ed. T. A. Skotheim, New York, Marcel Dekker, (1986).
4. W. Bantikassegn and O. Inganas, *Thin Solid Films*, **293** (1997) 138.
5. G. Gustafsson, M. Sundberg, O. Inganas and C. Svensson, *J. Mol. Elect.,* **6** (1990) 105.
6. W. Bantikassegn and O. Inganas, *J. Phys. D: Appl. Phy.*, **29** (1996) 2971.
7. W. Bantikassegn and O. Inganas, *Synth. Met.*, **87** (1997) 5.
8. C. S. Kuo, F. G. Wakim, S. K. Sengupta and S. K. Tripathy, *Jpn. J. Appl. Phys.*, **33** (1994) 2629.
9. D. Braun, and A. J. Heeger, *Appl. Phys. Lett.*, **58** (1991) 1982.
10. P. Dyreklev, G. Gustafsson, O. Inganas and H. Stubb, *Solid State Comm.*, **82** (1992) 317.
11. L. S. Roman, Wendimagen M., L. A. A. Pettersson, M. R. Andersson and O. Inganas, *Adv. Mat.*, **10** (1998) 10.
12. T. Yohannes, and O. Inganas, *Synth. Met.*, **107** (1999) 97.
13. N. Camaioni, G. Casalbore-Miceli, and G. Beggiato, *Synth. Met.*, **104** (1999) 169.

14. J.W. Gardner and T. T. Tan, *J. Phys., Condens. Matt.*, 1(1989) SB133.

15. N. Camaini, G. Casalbore-Miceli, A. Geri, F. Croce and F. Ronci, *Synth. Met.*, **88** (1997) 197.

16. S. Miyauchi, A. Fucki, Y. Sorimachi and I. Tsubata, *Synth. Met.*, **28** (1989) C691.

17. P.N. Bartlett, J. W. Gardner and R.G. Whitaker, *Sensors and Actuators*, A **23** (1990) 911.

18. C. Li, Y. Wang, M. Wan and S. Li, Synth. *Met.*, **39** (1990) 91.

19. S.A. Chen and Y. Fang, *Synth. Met.*, **609** (1993) 215.

20. Girma G. and Bantikasegn W. *SINET.*, **22** (1) (1999) 1.

21. F. W. Billmeyer, T*extbook of Polymer Science,* John Wiley & Sons, Inc., New York, (1971).

22. S. Roth, *One-Dimensional Metals*, VCH publishing, Inc. New York, NY, (1995).

23. H. Naarmann, *Synth. Met.*, **17** (1987) 223.

24. R.J. Ovellette and J. D. Rawn, *Organic Chemistry*, Mech. Inc. New York, (1994).

25. R. E. Peierls, *Quantum Theory of Solids*, Clarendon, Oxford, (1955).

26. J.E. Frommer and R.R. Chance, *Encyclopedia of Polymer Science and Engineering*, Wiley, New York, **5** (1986) 462.

27. J. L. Bredas, R. R. Chance, and R. Silbey, *Mol. Crys., Lig. Cryst.*, **77** (1981) 319.

28. H. C. Longuet-Higgeins and L. Salem, *Proc. R. Soc.*, A **251** (1959) 172.

29. J. A. Pople and S. H. Walmsley, *Mol. Phys.* **5** (1962) 15.

30. L. Salem, *The Molecular Orbital Theory of Conjugated Polymers*, Benjamin, New York, 1966.

31. N. Basescu, Z.-X. Liv, D. Moses, H. Naarmann, and N. Theophilou, *Nature.*, **327** (1987) 403.

32. J. S. Russel, *Proc. Roy. Soc.*, Edinburg, (1844).

33. C. J. Kupper and G.O. Whitfield, eds., *Pollarons* and *excitons*, Plenum, NY., (1963).

34. J. L. Bredas, B. Themans, J.G. Fripiat, J.M. Andre and R.R. Chance. *Phy. Rev.,* B **26** (1982) 5843.

35. Y. Onodera, *Phys. Rev.*, B **30** (1984) 301.

36. J. L. Beredas, J. C. Scott, K. Yakushi and G. B. Street, *Phys. Rev.*, B**30** (2) (1984) 1023.

37. Bantikassegn Workalemahu, *Ph.D Dissertation*, ISBN 91-7871-581-4, Linkoping University, Sweden, 1996.

38. J. J. Ritsko, *Phys. Rev. Lett.* **46** (1981) 849.

39. A. J. Heeger, S. Kivelson, J. R. Schrieffer and W. -P. Su, *Rev. mod. Phys.*, **60** (3) (1988) 782.

40. E. Punkka and M. F. Rubner, J. D. Hettinger and J.S. Brooks, S.T. Hannahs. *Phy. Rev.,* B **43** (11) (1991) 9076.

41. Y. –W. Park, A. J. Heeger, M. A. Druy and A. G. MacDiarmid, J. Chem. Phys., **75** (1980) 946

42. A. B. Kaiser, *Electronic Properties of Conjugated Polymers*, ed. H. Kuzmany, M. Mehring, S. Roth, Heidelberg: Springer Verlag, (1987).

43. P. Sheng, and J. Klafter, *Phy. Rev.,* B **27** (1983) 2583.

44. N. F. Mott and E.A. Davis, *Electric Processes in Non-Crystalline Materials*, 2nd ed., Clarendon Press, Oxford, (1979).

45. S. Kivlson, *Phys. Rev.* B **25** (1982) 3798.

46. I. Youm, M. Cadene and D. Laplaze, *J. Mat. Sci. Let.*, **14** (1995) 1712.

47. P. Sheng, E. K. Sichel, and J. L. Gittleman, *Phys. Rev. Lett.*, **40** (1978) 1197.

48. P. Sheng, *Phy. Rev.,* B **21** (1980) 2180.

49. E. S. Yang, *Fundamentals of Semiconductor Devices*, McGraw-Hill, Inc., New York, (1992).

50. S. M. Sze, *Physics of Semiconductor Devices*, John Wiley & Sons, Inc., New York, (1981).

51. E.H. Rhoderick, and R. H. Williams, *Metal-Semiconductor Contacts*, 2nd ed., Oxford University Press, New York, (1988).

52. T. A. Skotheim, R. I. Elesenbaumer and J. R. Reynolds, *Handbook of Conducting Polymers*, Marcel Dekker, Inc., (1998).

53. J. Mijovic and F. Bellucci, *Impedance Spectroscopy of Reactive Polymers, Review Article, TRIP.*, **4** (3) (1996) 74.

54. Bantikassegn W., *Bull., Chem. Soc. Ethiop.*, **13** (2) (1999) 143.